Journal of Animal & Plant Sciences, 36(1): 2026, Page: 237-247
ISSN (print): 1018-7081; ISSN (online): 2309-8694
https://doi.org/10.36899/JAPS.2026.1.0020

MECHANISM OF RETIGABINE-MEDIATED TLR4-TRIF PATHWAY ON THE INFLAMMATORY RESPONSE IN RATS WITH ISCHEMIC STROKE

M. Li[1], J. Zhao[2] and A.H. Li[3*]

[1]Department of Neurology, Nantong University School of Medicine, Nantong, 226000, Jiangsu, China;
[2]Department of Neurology, Nantong RICH Hospital, Nantong, 226000, Jiangsu, China;
[3]Department of Neurology, Affiliated Hospital of Nantong University, Nantong, 226000, Jiangsu, China.
[*]Corresponding author Email: liaihongahnu@163.com

ABSTRACT

Ischemic stroke (IS) leads to cerebral tissue hypoxia and energy disruption due to the interruption of cerebral blood flow, which induces cellular damage and inflammation. This study was to investigate whether retigabine (RET) alleviates brain inflammation in IS rats by modulating the Toll-like receptor 4-TIR domain-containing adaptor inducing interferon (IFN)-beta (TLR4-TRIF) pathway and explores the underlying mechanisms. Rat hippocampal neurons (HT22) were divided into Group A (blank control), Group B (H_2O_2-induced hypoxia for 1 hour), and Group C (treatment with 5 μg/mL RET after H_2O_2 exposure). Cell viability was measured using the 3-(4,5-dimethylthiazol-2-yl)-2,5-diphenyltetrazolium bromide (MTT) assay, and inflammatory cytokines were detected by enzyme-linked immunosorbent assay (ELISA). Additionally, cell apoptosis and reactive oxygen species (ROS) levels were assessed. Rats were further Assigned to sham surgery group, IS model group (middle cerebral artery occlusion via the filament method), and RET group (intraperitoneal injection of 5 mg/kg RET 1-hour post-surgery). Comparative endpoints included neurological function scores, infarct volume, brain inflammatory cytokines, and protein expression of the TLR4-TRIF pathway. Cell viability in Group B and Group C was dramatically reduced versus Group A ($P \leq 0.05$). However, versus Group B, Group C exhibited an increase in cell survival, with reduced apoptosis, ROS, tumor necrosis factor (TNF)-α), and interleukin (IL)-1β levels ($P \leq 0.05$). Additionally, both IS group and RET group had higher neurological function scores and infarct volumes versus sham group ($P \leq 0.05$). RET group showed a prominent reduction in these parameters versus model group. Moreover, TNF-α, C-reactive protein, IL-6, and expressions of TLR4, TRIF, TRIF-related adaptor molecules, IFN regulatory factor 3, and IFN-beta proteins were all markedly decreased in RET group (all $P \leq 0.05$). RET exerts neuroprotective effects by inhibiting TLR4-TRIF signaling, thereby alleviating brain inflammation induced by IS.

Key words: Retigabine; TLR4-TRIF pathway; ischemic stroke; inflammatory response; mechanism

Published first online December 05, 2025 Published final January 20, 2026

INTRODUCTION

Ischemic stroke (IS) is a clinically acute illness induced by a significant disruption of cerebral blood flow, with a high rate of disability and mortality (Mendelson *et al*., 2021). The pathological mechanisms of IS are complex, involving multiple cellular and molecular interactions. Brain inflammation plays a dual role in the pathogenesis of IS: moderate inflammation helps clear damaged tissue and promotes repair, whereas excessive or prolonged inflammation exacerbates neuronal damage and leads to cell death (Huang *et al*., 2022; Lin *et al*., 2023). Vascular occlusion leads to cerebral hypoxia and ischemia, triggering nerve cell damage and an inflammatory response that not only participates in neuronal apoptosis but also exacerbates brain tissue damage during the pathogenesis of IS (Qiu *et al*., 2021; Aznaourova *et al*., 2020).

The Toll-like receptor 4 (TLR4) and its downstream adaptor protein TIR domain-containing adaptor inducing interferon (IFN)-beta (TRIF) (TLR4-TRIF) signaling plays a crucial role in regulating neuroinflammatory responses following ischemia (Song *et al*., 2022). Activation of this pathway triggers the transcription factors nuclear factor-kappa B (NF-κB) and IFN regulatory factor 3 (IRF3), which promote pro-inflammatory cytokine and chemokine expression, representing an important mechanism for pathogen recognition and immune response initiation (Yang *et al*., 2020; Deveci Ozkan *et al*., 2020). Therefore, the activity of the TLR4-TRIF pathway has a significant impact on the inflammatory response following IS.

Retigabine (RET) is an anticonvulsant that effectively reduces epileptic seizures of patients (Nass *et al*., 2016; Zahra *et al*., 2023; Janicki *et al*., 2019). Recent studies demonstrated that RET has significant

neuroprotective effects in IS. It exerts its effects by activating the potassium channel subfamily Q member (KCNQ) channels, regulating neuronal resting membrane potential, reducing excitotoxicity, and protecting neurons from ischemic damage (Morisaki *et al*., 2022; Maqoud *et al*., 2022; Clement *et al*., 2023). Additionally, RET has been shown to reduce reactive oxygen species (ROS) production, alleviating oxidative stress damage (Yokoyama *et al*., 2019), and suppress the release of inflammatory mediators, thereby reducing inflammation-induced neuronal injury (Barker *et al*., 2021; Wei *et al*., 2019). Although some studies suggest that RET may influence TLR4 pathway to regulate inflammatory responses, there is currently no direct evidence confirming its action through this pathway, especially in stroke models, and its underlying mechanisms remain to be further investigated.

In summary, this work investigated regulatory effects of RET on TLR4-TRIF signaling and inflammatory responses in an IS cell model. It was hypothesized that RET may inhibit this signaling, reduce the expression of inflammatory factors, alleviate post-stroke inflammation, and exert neuroprotective effects. Through *in vitro* and animal experiments, the study validated the effect of RET in modulating the TLR4-TRIF pathway and assessed its potential in mitigating neuroinflammation and protecting neuronal cells. The findings were expected to provide scientific evidence for therapeutic strategies in stroke treatment.

MATERIALS AND METHODS

Preparation of RET solution: The standard solution was prepared using the following procedures. Firstly, 100 mg of RET standard (Millipore Sigma, USA) was accurately weighed and positioned in a 100 mL measuring flask, dissolved with a blank solution (acetonitrile; Sinopharm Pharmaceutical Co., Ltd., China): water = 7:3) (Meirinho *et al*., 2021) and diluted to 1,000 μg·mL-1 for subsequent use. Next, 1 mL of the control stock solution was carefully taken with a 10 mL flask and diluted to 100 μg·mL-1 with a blank solution.

The test solution was prepared with the following operations. 150 mg of RET API (Jiangxi Ruiwei Biotechnology Co., Ltd., China) was accurately weighed and positioned in a 50 mL volumetric flask. Methanol (Sinopharm Pharmaceutical Co., Ltd., China) was used as a solvent to dissolve and ensure that the final volume was adjusted to the scale mark. The sample solution was prepared at 3 mg/mL and then further diluted with a drug-free blank solution, aiming for a concentration of 100 μg·mL-1.

High-performance liquid chromatography (HPLC) (Agilent, USA) detection was implemented as follows: Agilent ZOBAX SB-C18 column (150×4.6 mm, 3.5 μm); mobile phase A: gradient elution, 10 mmol/L sodium dihydrogen phosphate (SDP) (Sinopharm Pharmaceutical Co., Ltd., China), pH adjustment (potential of hydrogen) 2.5, filtration and degassing, mobile phase. The gradient elution program was 0-5 min: B phase increased from 10% to 50%; 5-10 min: maintained at 50%; 10-15 min: B phase increased from 50% to 90%; 15-20 min: maintained at 90%; 20-25 min: B phase returned to 10%. The flow rate was 1.0 mL/min, at 25°C. Injection volume was 10 μL.

Following operations were taken to determine the RET content. 5 test solutions made in different batches were selected for determination, and the content was calculated according to the external standard method.

In *vitro* experiments

Cells culture and grouping: The rat hippocampal neuron (HT22) cells (Wuhan Prosa Life Science & Technology Co., Ltd., China), which have been certified by Short Tandem Repeat genotype test report, were placed in a flask of Roswell Park Memorial Institute 1640 medium (Merck KGaA, Germany) comprising 10% fetal bovine serum (FBS) for culture in a 5% CO_2 at 37°C. Subsequently, they were digested with 0.25% trypsin (Shanghai Jingchun Biochemical Technology Co., Ltd., China) after attached and covered with the bottom of the bottle.

The cells were groups into group A (blank group), B (hypoxia group), and C (Hypoxia + RET intervention group), with three replicates per group.

Cell model construction: The well-maintained HT22 cells were adjusted to a concentration of 1×10^5/mL and seeded into 96-well plates (100 μL/well). After 24 hours of incubation, Group A received blank culture medium, while Group B and Group C were treated with culture medium containing 100 μM H_2O_2 for 1 hour. Subsequently, Group C was further incubated with RET (5 μg/mL) for 1 hour, and Group A and Group B were treated with an equal volume of physiological saline as controls.

Cell model evaluation: (1) Detection of cell viability: 3-(4,5)-dimethylthiahiazo (-z-y1)-3,5-di-phenytetrazoliumromide (MTT) (Wuhan Proxel Life Science & Technology Co., Ltd., China) method was adopted. After modeling, 20 μL of MTT solution (5 mg/mL) was introduced and subsequently positioned in a 37°C, 5% CO_2 for 4 h. After supernatant discarding, 200 μL of Dimethyl sulfoxide (DMSO) solution was introduced, and the resulting mixed solution was put on a cell shaker for 10 min to fully dissolve. Optical density value at 570 nm was determined and recorded.

(2) Apoptosis detection: after modeling, 1 mL of Phosphate Buffered Saline (PBS) was mixed to wash the cells twice. After PBS removal, 400 μL binding buffer (1 ×) and 2 μL of Annexin (Wuhan Proxel Life Science & Technology Co., Ltd., China) V-FITC were introduced in

turn for a purpose of incubating them for 10 min. Following that, 2 μL of PI dye was dropped to allow a reaction for 5 min. At this time, cells were observed and photographed under a fluorescence microscope (Alluxa, USA).

(3) Detection of intracellular ROS level: After modeling, HT22 cells were treated by removing the original culture medium and washing the cells twice with serum-free and anti-antibody Dulbecco's Modified Eagle Medium in preparation for the determination of intracellular ROS levels. Subsequently, the final concentration of 5 μM fluorescent probe dichloro-dihydro-fluorescein diacetate (Shanghai Maokang Biotechnology Co., Ltd., China) working solution was introduced to let them incubate at 37°C in the dark for 20 - 30 min. At this time, it can observe and photograph under a fluorescence microscope.

(4) Cytokine levels were measured to assess the cellular inflammatory response. The supernatants from each group were collected and centrifuged at 4° C, 3000 rpm for 10 minutes. The resulting supernatants were then analyzed using enzyme-linked immunosorbent assay (ELISA) kits (Thermo Fisher Scientific, USA) to measure the concentrations of pro-inflammatory cytokines tumor necrosis factor (TNF)-α and interleukin (IL)-1β. The procedures were performed regarding instructions provided by the ELISA kit.

In *vivo* experiments

Animals and grouping: Thirty specific pathogen free-grade healthy male Sprague-Dawley rats (aged 8 weeks with body weight of 240~260 g; Jintai Meidi Biotechnology Co., Ltd., China) were enrolled in this study and kept in standard animal houses. Animal experiments were approved by the Ethics Committee of Affiliated Hospital of Nantong University, complied with animal management regulations.

Rats were adaptively fed for one week, after which 10 rats were selected randomly as sham group. The remaining 20 rats underwent the left middle cerebral artery occlusion (MCAO) surgery. After successful modeling, they were divided into model group and RET group, each consisting of 10 rats. The sham group underwent a sham operation, which was identical to model group's operation except for not ligating the vessels and not inserting the suture occlusion. RET group was treated with RET after the construction of the MCAO model, while sham group and the model group were given an equal amount of physiological saline. The average body weights of the rats in sham group, model group, and RET group were 251.03 ± 8.03 g, 252.22 ± 10.17 g, and 249.84 ± 9.96 g, respectively. There were no statistically significant differences in the average body weights of the rats among the groups (P>0.05).

IS model construction: The middle cerebral artery occlusion model in rats was induced using the filament insertion method (Li *et al.*, 2021). Anesthesia was administered intraperitoneally with sodium pentobarbital at 30 mg/kg. Subsequently, the rat was secured in a supine position on the operating table. The skin in the anterior midline region of the rat neck was prepared, disinfected with 75% alcohol. A longitudinal incision (1.5 cm) was performed on median line of neck of the rat, and the muscle and fascia tissues distributed along the line were carefully separated to reveal the triangular region of neck composed of right common carotid artery, lateral carotid artery, and medial carotid artery. Next, it would carefully separate and expose the three vessels. The procedure continued. The proximal end of right common carotid artery was clamped and the subtle branches of right lateral carotid artery were carefully dissociated with bipolar electrocoagulation (Shanghai Yuyan Scientific Instrument Co., Ltd., China). Subsequently, the distal end of the right lateral carotid artery was ligated and cut approximately 3 mm below its branch point. After that, the right internal carotid artery was clamped, a small incision of about 0.2mm was cut at the stump of the right external carotid artery at an angle of 45 degrees, and the wire plug (Yushun Biotechnology Co., Ltd., China) was marked at a distance of 1.0cm from the apex, the arterial clamp was loosened, and the wire plug was inserted into the internal segment of the right internal carotid artery in an upward and inward direction. The plug length was 1 cm from the bifurcation of the vessel, and if the plug was pushed inward, there would be slight resistance. After 1 hours of ischemia, the suture occlusion was extracted to achieve reperfusion. Finally, the securing suture for the ligature was tied tightly, the loose end of the ligature was cut, and the incision was sutured. Appropriate heat preservation measures were maintained to ensure stable body temperature during operation and postoperative recovery. After the procedure, the rats were safely back to their habitat and allowed free access to both food and water, ensuring adequate post-operative care. In sham group, no ligature was inserted, and all other procedures were identical.

Intervention methods: RET at 5 mg/kg was intraperitoneally injected into RET group 1 h after surgery, and animals in the other groups were intraperitoneally administrated with the same amount of normal saline.

During the stroke model surgery, an appropriate dosage of anesthetics was administered, and the animal's respiratory rate and blood oxygen saturation were monitored to ensure adequate anesthetic depth, avoiding both over-anesthesia and insufficient anesthesia. Throughout the procedure, a heating pad was used to maintain the animal's body temperature within the normal range (approximately 37°C) to prevent the effects of hypothermia on experimental results. Postoperatively,

the animals' vital signs, including respiration, heart rate, and body temperature, were closely monitored, and necessary supportive treatments, such as fluid and electrolyte supplementation, were provided to ensure proper recovery.

Animal model evaluation: (1) Neurological deficit scores: assessed 24 hours postoperatively when the rats were awake and under quiet conditions. They were scored according to following criteria: 0 points: no neurological deficits; 1 point: being unable to completely extend the contralateral forelimb when tail-pulled; 2 points: circling towards the contralateral side during walking; 3 points: falling towards the contralateral side during walking; and 4 points: being unable to walk or loss of consciousness.

2) Sample selection: chloral hydrate anesthetized rats were given PBS cardiac perfusion, and the brain was quickly decapitated after the liver discolored, and it was quick-frozen in a -20 °C refrigerator for future use.

(3) Infarct volume detection: the frozen brain tissue was sliced along the coronal plane into 5 sections, each approximately 1 mm thick. These sections were placed in a culture dish in the same orientation, and a solution with a concentration of 2% triphenyltetrazolium chloride (TTC) (Shanghai Aladdin Biochemical Technology Co., Ltd., China) was added. The dish was then incubated in a light-avoiding, constant-temperature chamber at 37°C for 15-20 minutes. Normal brain tissue appeared fresh red, while the infarcted brain area appeared white. The brain tissue sections were then immobilized in 4% paraformaldehyde solution (Merck KGaA, Germany). After 24 hours of fixation, the slices were photographed and recorded, and proportion of infarct area was measured through image analysis software system. The percentage of infarct volume was determined by calculating the cumulative value of the infarct area in all sections, dividing by the sum of the total area of all brain sections, and multiplying by 100%.

(4) Hematoxylin and eosin (H&E) staining (Feijing Biotechnology Co., Ltd., China) of brain tissue: partial brain tissue was immersed in a 10% formalin solution for fixation for 24 h. After routine gradient dehydration, transparency, and paraffin embedding, brain tissue paraffin sections were prepared. 4 μm thick paraffin section was taken, and after deparaffinization, hydration in ethanol, and washing, it underwent gradual staining with hematoxylin and eosin. Excess staining solution was cleared, and subsequently these sections were sealed with neutral resin. Morphological alterations in brain tissue were examined using an optical microscope (Keyence, Japan).

ELISA detection: The rat brain tissue was removed from the refrigerator, ground into a homogenate, then put into a centrifuge tube for 10-min centrifugation at 4,000 r/min. Contents of TNF-α, C-reactive protein (CRP), and IL-6 in supernatant of rat brain cells were detected through ELISA kit.

Detection of TLR4-TRIF signaling-associated proteins: Western blotting detected the specific structural molecules of TLR4-TRIF signaling and the mRNA expressions in key cytokines, like TLR4, TRIF-related adaptor molecule (TRAM), IFN regulatory factor 3 (IRF-3), and INF-β.

After mixing 1 mL of lysis buffer with 10 μL of 100 mM phenylmethanesulfonyl fluoride (highly toxic) (Selleck, China), the mixture was placed on ice for later use. Rat brain tissue was retrieved from the refrigerator and homogenized to form a uniform paste. The paste was then transferred to a centrifuge tube, positioned in a centrifuge (Thermo Fisher Scientific, USA) at 4,000 rpm for 10 minutes, and the residual liquid was aspirated using a pipette (Brand, Germany). To each tube, 400 μL of lysis buffer containing phenylmethylsulfonyl fluoride was introduced, and the resulting blended solution was lysed on ice for 30 minutes. After thorough lysis, these samples were underwent centrifugation at 4°C, 12,000 rpm for 5 minutes. Protein quantification was performed following the instructions of the bicinchoninic acid assay (Changsha Abvi Biotechnology Co., Ltd., China) protein quantification kit. Finally, the bands after visualization were saved as computer files, and ImagePro Plus analysis was utilized to digitize and analyze the grayscale values of each specific band on the images. The protein content (%) was computed as IOD (target protein) / IOD (internal reference) × 100% (*IOD - Impact on Demand).

Statistical analysis: Data were analyzed using IBM *SPSS 23.0*. Continuous variables conforming to a normal distribution were denoted as mean ± standard deviation, and One-way ANOVA was employed for analysis. Inter-group comparisons were conducted using the least significant difference method. In multi-group comparisons, the Bonferroni correction method was adopted to control the overall error rate. $P \leq 0.05$ meant statistically significant difference.

RESULTS

Results of RET solution evaluation: The HPLC results were presented in Fig. 1A and Fig. 1B. It was evident that the RET solution prepared exhibited chromatographic peaks that were essentially consistent with the RET standard. Additionally, the RET content in solution samples from 5 different batches was compared, with results demonstrated in Fig. 1C. The observations indicated that the RET content in the solution exceeded 99.5%, and the relative standard deviation was consistently below 5%, meeting the specified standards.

In *vitro* test results

Results of cell model evaluation: Cell viability analysis showed that, versus Group A (96.77±6.23%), the cell survival rates in Group B (61.46±5.14%) and Group C (82.75±5.84%) were substantially reduced, with Group C being markedly superior to Group B (all $P \leq 0.05$) (Fig. 2A). Apoptosis detection revealed that, versus Group A (1.83 ± 0.14%), the apoptosis rates in Group B (18.64 ± 1.56%) and Group C (12.65 ± 2.11%) were greatly increased, with Group B notably surppassing Group C (all $P \leq 0.05$) (Fig. 2B). ROS level analysis indicated that, versus Group A (12.63±2.11), the ROS levels in Group B (46.24 ± 3.55) and Group C (27.13 ± 2.19) were dramatically elevated (all $P \leq 0.05$) (Fig. 2C). Furthermore, versus Group A, inflammatory factor levels (TNF-α, IL-1β) were drastically higher in Group B and Group C, but the levels in Group C were notably inferior to Group B (all $P \leq 0.05$) (Fig. 2D).

Results of *in vivo* experiments

Rat model construction results: Neurological deficit score analysis revealed that, versus sham group (0.00 ± 0.00), both model group (3.22 ± 0.79) and RET group (2.16 ± 0.64) had markedly higher scores (both $P \leq 0.05$), with RET group showing a drastically lower score than model group ($P \leq 0.05$) (Fig. 3A). Cerebral infarct volume analysis demonstrated that, versus sham group (0.00 ± 0.00%), both model group (68.74% ± 5.14%) and RET group (42.37% ± 3.54%) had notably larger infarct volumes (both $P \leq 0.05$), with RET group showing a substantially smaller infarct volume than model group ($P \leq 0.05$) (Fig. 3B). H&E staining showed that rat brain tissue in sham group had normal cell structure, no edema, clear nuclear boundary, swelling, widening gap, and abnormal irregular shape in model group. Compared with model group, RET group performed significantly better, with reduced edema and narrowed gap, as shown in Fig. 3C.

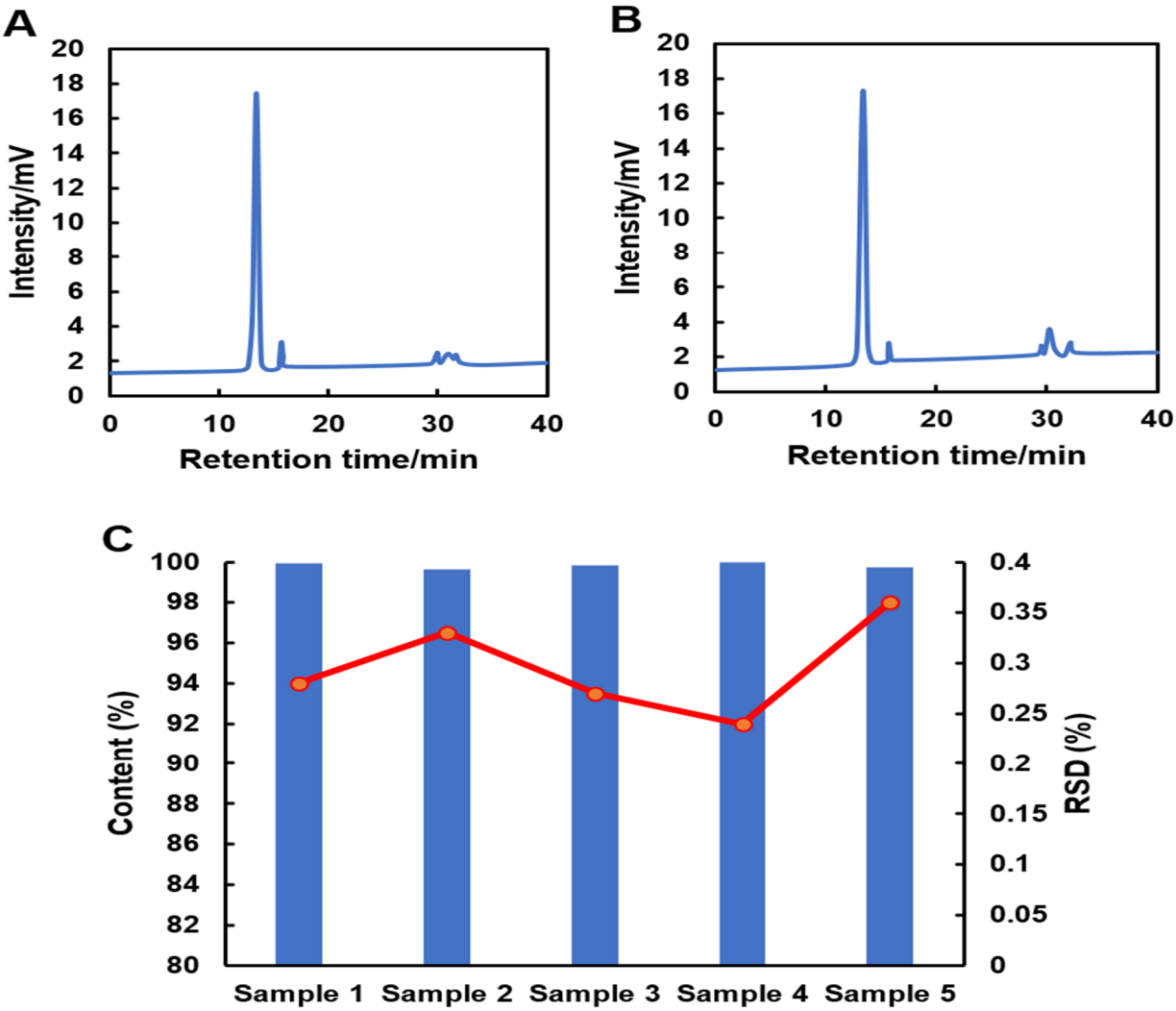

Fig. 1. HPLC results. A: standard solution; B: test solution; C: detected content.

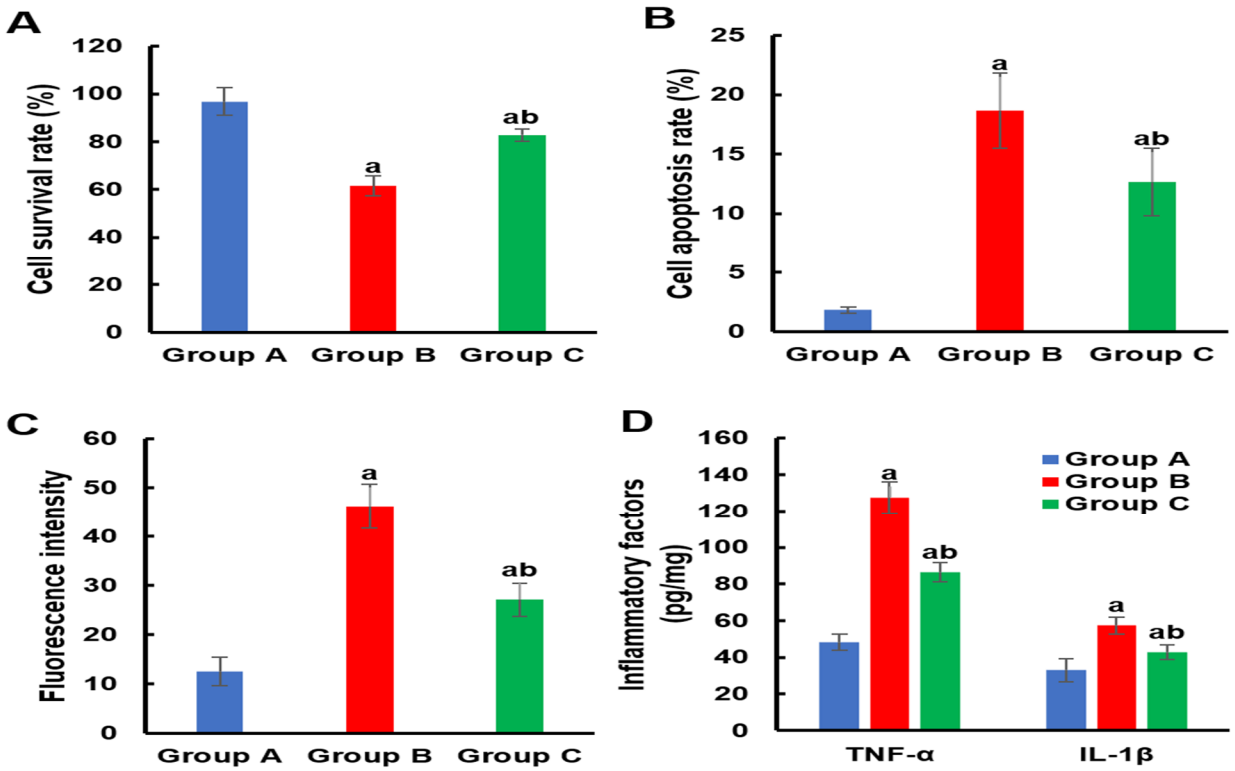

Fig. 2. Cellular survival rate assay results. A: cellular survival rate; B: cellular apoptosis rate; C: reactive oxygen species (ROS) level; D: inflammatory factor level.

Note: [a]*P*≤0.05 vs. group A; [b]*P*≤0.05 vs. group B.

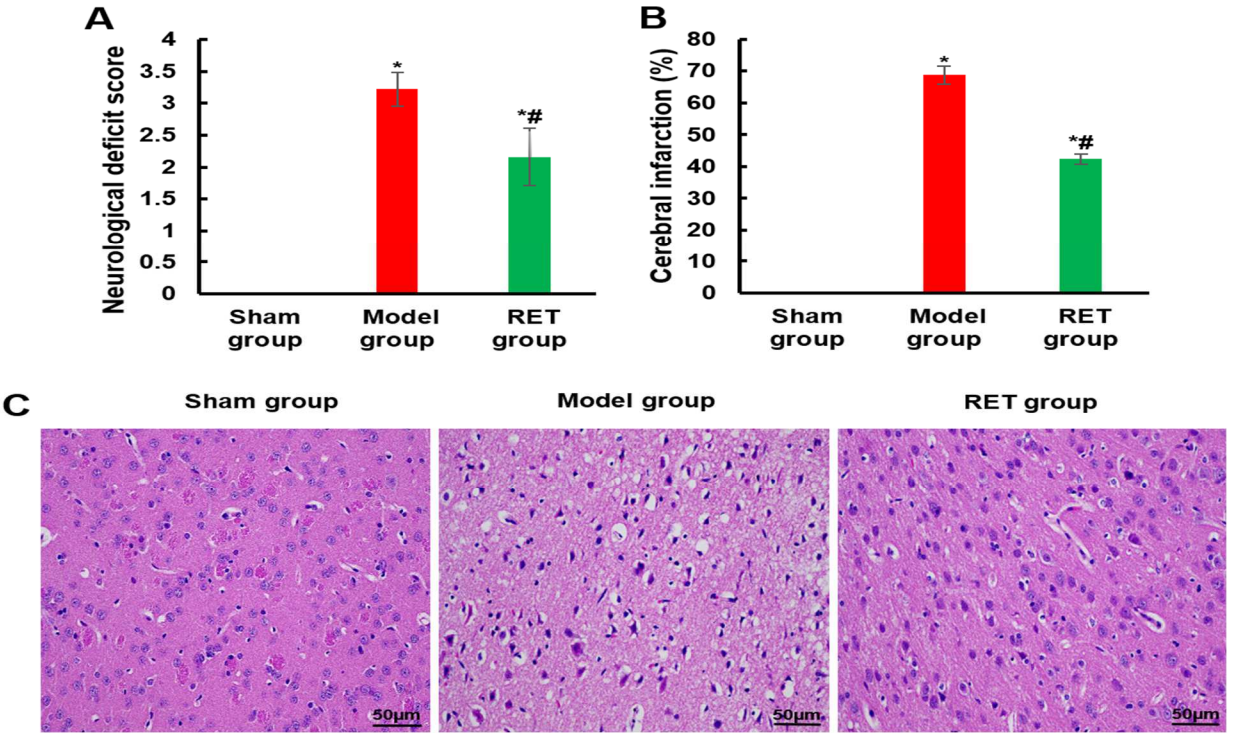

Fig.3. Comparison of rat models in distinct group. A: neurological deficit scores; B: infarct volume; C: H&E staining (×200).

Note: [*]*P*≤0.05 vs. sham group; [#]*P*≤0.05 vs. model group.

Detection results of inflammatory factor levels in rat brain cells: In sham group, TNF-α, CRP, and IL-6 in the brain tissue of rats were 47.62 ± 5.84 pg/mL, 6.02 ± 1.17 mg/L, and 33.64 ± 2.54 pg/mL, respectively. In model group, these levels were markedly elevated, reaching 74.35 ± 3.26 pg/mL, 7.88 ± 1.41 mg/L, and 44.72 ± 2.59 pg/mL (all $P \leq 0.05$). In RET group, the levels were considerably reduced versus model group, with values of 62.41 ± 8.29 pg/mL, 6.83 ± 0.98 mg/L, and 38.59 ± 1.92 pg/mL (all $P \leq 0.05$) (Fig. 4).

Detected TLR4-TRIF signaling-related proteins in rat brain cells: Western blot analysis revealed that, versus sham group, protein TLR4, TRIF, TRAM, IRF-3, and IFN-β levels were substantially elevated in both model Group and RET group ($P \leq 0.05$). In comparison to model group, these protein expressions were notably reduced in RET group ($P \leq 0.05$) (Fig. 5).

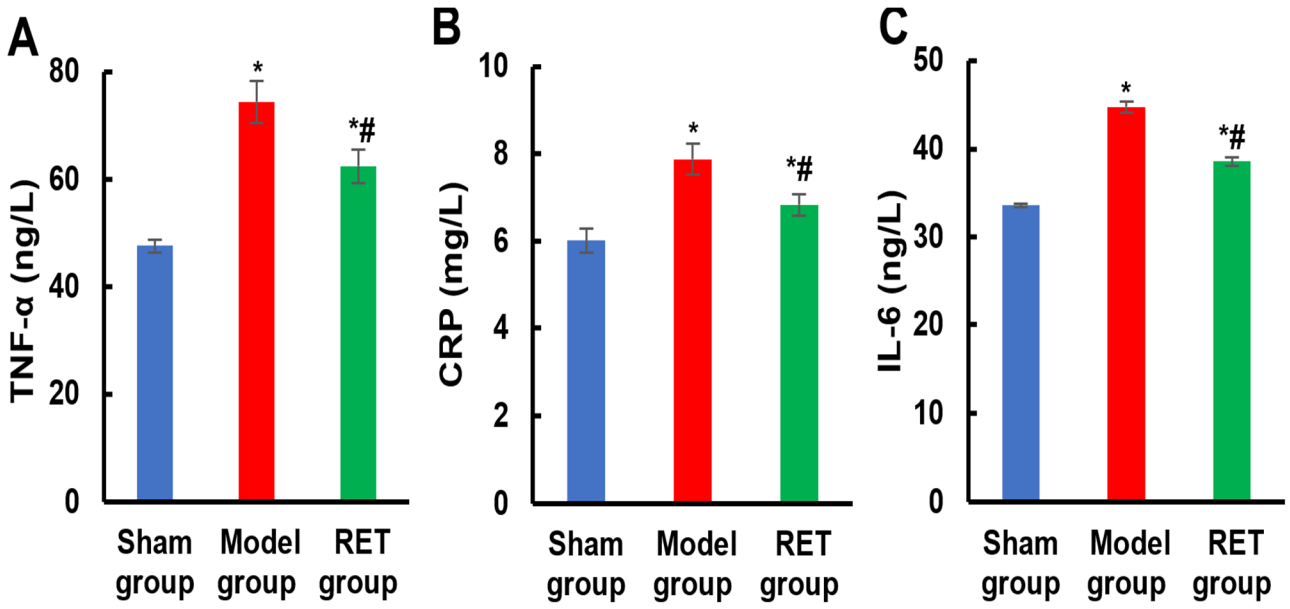

Fig. 4. Comparison of inflammatory factor levels. A: TNF-α; B: CRP; C: IL-6.
Note: $^{*}P \leq 0.05$ vs. sham group; $^{\#}P \leq 0.05$ vs. model group.

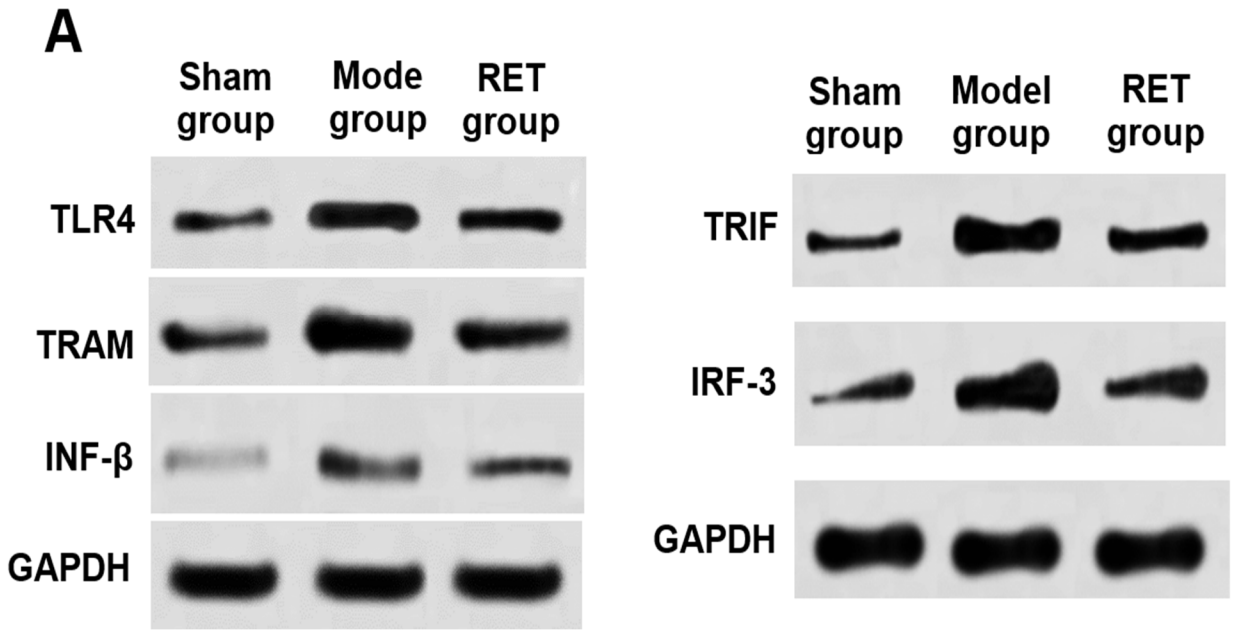

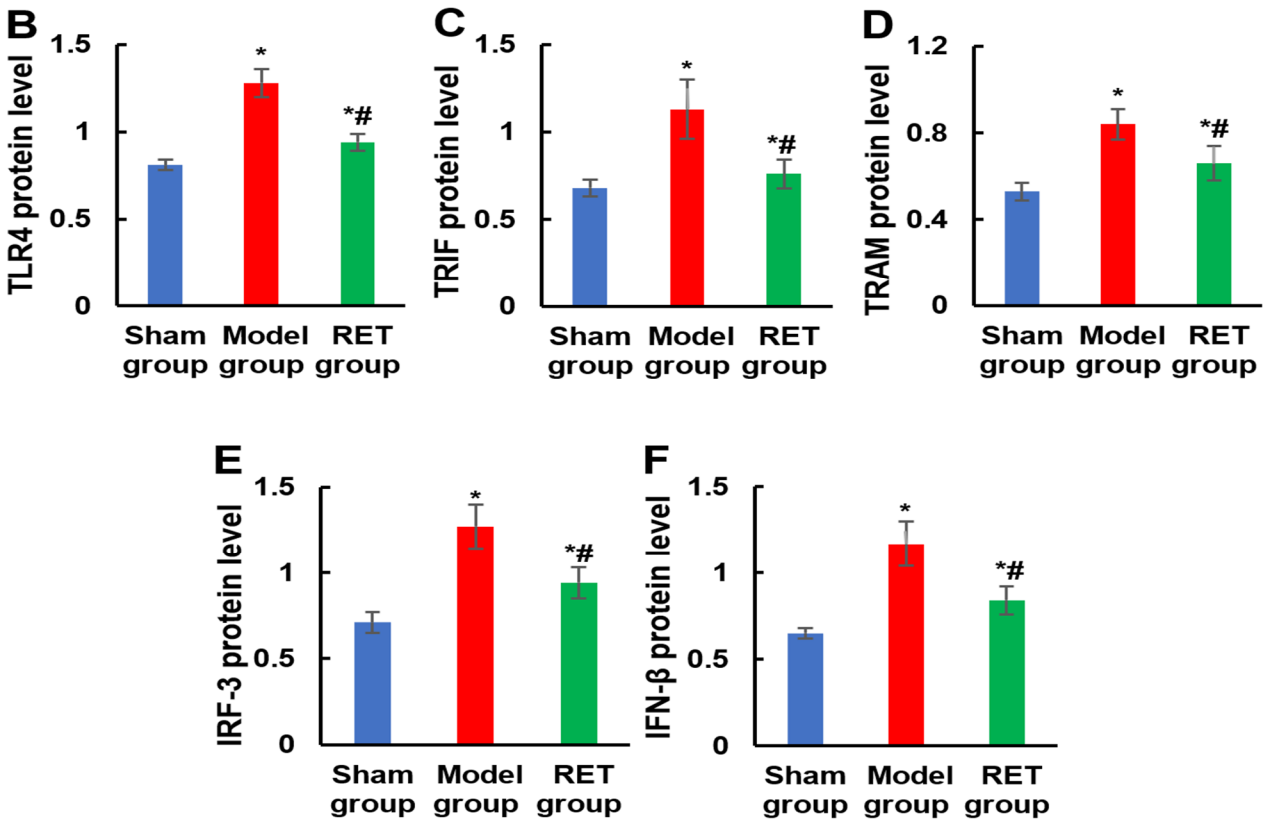

Fig. 5. Changes in levels of TLR4-TRIF signaling-associated proteins. A: Western blotting band; B: TLR4; C: TRIF; D: TRAM; E: IRF-3; F: IFN-β.

Note: $^{*}P \leq 0.05$ vs. sham group; $^{\#}P \leq 0.05$ vs. model group.

DISCUSSION

The results indicated that RET solution has high purity and stability, significantly increasing cell viability under hypoxic conditions, reducing apoptosis and ROS levels, and inhibiting the release of inflammatory cytokines. In the animal model of IS, RET effectively reduced neurological deficit scores and cerebral infarct volume, alleviated brain edema and tissue pathological damage, and exerted significant neuroprotective effects by modulating the expression of proteins related to TLR4-TRIF pathway, thereby inhibiting the inflammatory response.

Furthermore, the results showed that the RET solution has a high purity (>99.5%) and good stability, meeting the experimental requirements, and the preparation method demonstrates good reproducibility. IS leads to disruption of blood supply, resulting in local brain areas being deprived of oxygen and nutrients, resulting in neuronal cell damage and death (Zhao *et al*., 2022; Li *et al*., 2023). In addition, IS induces inflammatory responses and triggers oxidative stress, resulting in elevated intracellular ROS levels (Koutsaliaris *et al*., 2022; Huang *et al*., 2022; Su *et al*., 2022). This mechanism is consistent with the significant increase in ROS levels observed in Group B and Group C of the *in vitro* hypoxic cell model, suggesting successful establishment of the hypoxia model. In this model, RET markedly increased cell viability under hypoxic conditions, reduced apoptosis, modulated ROS levels, and effectively inhibited the release of inflammatory cytokines, indicating its positive inhibitory effect on stroke-related inflammation.

After modeling, the neurological deficit scores and infarct volume in model group were markedly increased ($P \leq 0.05$), while RET group showed a significant reduction versus the model group ($P \leq 0.05$), suggesting that RET has potential neuroprotective effects (Zhou *et al*., 2021; Yu *et al*., 2022). The brain tissue of the model group exhibited typical IS pathological features, such as cell swelling, expanded interstitial spaces, and morphological abnormalities (Shi *et al*., 2022; Liu *et al*., 2023; Xing *et al*., 2020). In contrast, RET group showed reduced edema, smaller tissue gaps, and significant pathological improvement. In addition, following results were obtained: in comparison to sham group, levels of inflammatory cytokines in brain tissue of rats in model group and RET group were significantly increased ($P \leq 0.05$), whereas those of inflammatory cytokines in RET group was significantly decreased

when compared with the condition in model group, demonstrating an obvious difference ($P \leq 0.05$). The increase in inflammatory cytokines in rat brain tissue cells is consistent with the pathological features of IS and aligns with the results observed in the *in vitro* experiments. TNF-α is mainly generated by activated immune cells to induce local inflammatory response, leading to lesions and tissue damage (Jang *et al*., 2021). CRP is synthesized by the liver and can increase rapidly in response to inflammation or infection, thus playing a key role in the inflammatory process by enhancing the phagocytosis of macrophages against bacteria and dead cells (Levinson *et al*., 2022). IL-6 serves as a regulator of immune response and inflammation, and can promote B cell differentiation and T cell proliferation (Hirano, 2021). The decreased levels of inflammatory cytokines in RET rats brain tissue cells suggest that RET has a potential inhibitory effect on IS-induced inflammatory response. Recent studies have also shown that RET has anti-inflammatory properties, aligning with the observations in this study (Zhang *et al*., 2020; Citak *et al*., 2022).

Western blotting experiment results signified that RET group had lower levels of these proteins versus the model group. This suggests that these proteins are activated in the IS model. At the same time, these findings also suggest that they are involved in regulating inflammation and immune responses, specifically TLR4. Elevated levels of TLR4 may indicate neuronal damage during stroke, triggering an inflammatory response. Previous studies have demonstrated that TLR4 performs well in diagnosis (Liu *et al*., 2022; Chen *et al*., 2021). TRIF and TRAM are key molecules in TLR signaling pathway, and their elevation may reflect the activation of TLR signaling pathway, suggesting that there is an immune system response to the stroke model (Nilsen *et al*., 2015). Elevated levels of IFN IRF-3 and IFN-β suggest that the immune system releases more IFN after stroke to counteract inflammation and protect tissue (Chen *et al*., 2020; Wanve *et al*., 2019). The levels of these parameters in RET group were lower to those in model group, indicating that RET had a certain regulatory effect on the immune response in the IS model, thereby alleviating the overactivation of the immune system.

Although this study confirmed that RET exerts neuroprotective effects in the IS cell model by inhibiting apoptosis, oxidative stress, and inflammation through TLR4-TRIF pathway, it provides a theoretical foundation for its clinical application. However, the sample size of this study is relatively small, which may affect the power of statistical analysis and the generalizability of the results. Moreover, this study mainly focuses on cell and animal models, and clinical trials have not yet been conducted. In terms of confounding factors, this study may be subject to influences such as differences in animal models, cell line selection, and environmental factors. In future study, clinical trials will be considered to verify the safety and efficacy of RET in humans. Further exploration of the detailed mechanisms by which RET regulates TLR4-TRIF signaling, including changes at the molecular level and the regulatory pathways of the signal transduction, will be conducted to more comprehensively understand the mechanisms of action of RET.

Conclusion: Our results suggested that RET exerted an anti-inflammatory role in the IS cell model by modulating TLR4-TRIF signaling. The *in vitro* experiments signified RET effectively increased cellular survival rate and reduced apoptosis, ROS levels, and inflammatory factor levels. Conversely, the *in vivo* experiments revealed that RET reduced neurological deficit scores and infarct volume, reduced brain cell edema, and inhibited the release of inflammatory cytokines. In addition, RET further blocked the inflammatory response by inhibiting the molecular expression of TLR4-TRIF signaling, thereby acting as a protective effect on nerve cells. Therefore, RET may be a potential drug for IS treatment. Nevertheless, this study will be extended and deepened in future to validate the outcomes obtained here.

Author's contribution: Conception and study design: Mei Li and Aihong Li; data acquisition and analysis: Mei Li, Jing Zhao and Aihong Li; manuscript draft, editing and revision: Mei Li and Aihong Li. All authors approved the final manuscript.

Competing Interest: The authors have declared that no competing interest exists.

REFERENCES

Aznaourova, M., H. Janga, S. Sefried, A. Kaufmann, J. Dorna, S.M. Volkers, P. Georg, M. Lechner, J. Hoppe, S. Dökel, N. Schmerer, A.D. Gruber, U. Linne, S. Bauer, L.E. Sander, B. Schmeck and L.N. Schulte (2020). Noncoding RNA *MaIL1* is an integral component of the TLR4-TRIF pathway. Proc Natl Acad Sci U S A. 117(16): 9042-9053. DOI:10.1073/pnas.1920393117

Barker, B.S., J. Spampanato, H.S. McCarren, K. Berger, C.E. Jackson, D.T. Yeung, F.E. Dudek and J.H. McDonough (2021). The K_v7 Modulator, Retigabine, is an Efficacious Antiseizure Drug for Delayed Treatment of Organophosphate-induced Status Epilepticus. Neuroscience. 463: 143-158. DOI:10.1016/j. neuroscience.2021.03.029

Chen, G., L. Li and H. Tao (2021). Bioinformatics Identification of Ferroptosis-Related Biomarkers and Therapeutic Compounds in Ischemic Stroke. Front Neurol. 12: 745240. DOI:10.3389/fneur.2021.745240

Chen, K.H., K.C. Lin, S.F. Ko, J.Y. Chiang, J. Guo and H.K. Yip (2020). Melatonin against acute ischaemic stroke dependently via suppressing both inflammatory and oxidative stress downstream signallings. J Cell Mol Med. 24(18): 10402-10419. DOI:10.1111/jcmm.15654

Citak, A., E. Kilinc, I.E. Torun, S. Ankarali, Y. Dagistan and H. Yoldas (2022). The effects of certain TRP channels and voltage-gated KCNQ/Kv7 channel opener retigabine on calcitonin gene-related peptide release in the trigeminovascular system. Cephalalgia. 42(13): 1375-1386. DOI:10.1177/03331024221114773

Clement, A., S.L. Christensen, I. Jansen-Olesen, J. Olesen and S. Guo (2023). The ATP sensitive potassium channel (KATP) is a novel target for migraine drug development. Front Mol Neurosci. 16: 1182515. DOI:10.3389/fnmol.2023.1182515

Deveci Ozkan, A., S. Kaleli, H.I. Onen, M. Sarihan, G. Guney Eskiler, A. Kalayci Yigin and M. Akdogan (2020). Anti-inflammatory effects of nobiletin on TLR4/TRIF/IRF3 and TLR9/IRF7 signaling pathways in prostate cancer cells. Immunopharmacol Immunotoxicol. 42(2): 93-100. DOI:10.1080/08923973.2020.1725040

Hirano, T. (2021). IL-6 in inflammation, autoimmunity and cancer. Int Immunol. 33(3): 127-148. DOI:10.1093/intimm/dxaa078

Huang, G., J. Zang, L. He, H. Zhu, J. Huang, Z. Yuan, T. Chen and A. Xu (2022). Bioactive Nanoenzyme Reverses Oxidative Damage and Endoplasmic Reticulum Stress in Neurons under Ischemic Stroke. ACS Nano. 16(1): 431-452. DOI:10.1021/acsnano.1c07205

Huang, L., Y. Zhang, L. Zhao, Q. Chen and L. Li (2022). Ferrostatin-1 Polarizes Microglial Cells Toward M2 Phenotype to Alleviate Inflammation After Intracerebral Hemorrhage. Neurocrit Care. 36(3): 942-954. DOI:10.1007/s12028-021-01401-2

Janicki, P. K., C. Eyileten, V. Ruiz-Velasco, J. Pordzik, A. Czlonkowska, I. Kurkowska-Jastrzebska, S. Sugino, Y. Imamura Kawasawa, D. Mirowska-Guzel and M. Postula (2019). Increased burden of rare deleterious variants of the KCNQ1 gene in patients with large-vessel ischemic stroke. Mol Med Rep. 19(4): 3263-3272. DOI:10.3892/mmr.2019.9987

Jang, D. I., A. H. Lee, H. Y. Shin, H. R. Song, J. H. Park, T. B. Kang, S. R. Lee and S. H. Yang (2021). The Role of Tumor Necrosis Factor Alpha (TNF-α) in Autoimmune Disease and Current TNF-α Inhibitors in Therapeutics. Int J Mol Sci. 22(5): 2719. DOI:10.3390/ijms22052719

Koutsaliaris, I. K., I. C. Moschonas, L. M. Pechlivani, A. N. Tsouka and A. D. Tselepis (2022). Inflammation, Oxidative Stress, Vascular Aging and Atherosclerotic Ischemic Stroke. Curr Med Chem. 29(34): 5496-5509. DOI:10.2174/0929867328666210921161711

Levinson, T. and A. Wasserman (2022). C-Reactive Protein Velocity (CRPv) as a New Biomarker for the Early Detection of Acute Infection/Inflammation. Int J Mol Sci. 23(15): 8100. DOI:10.3390/ijms23158100

Li, Q., X. Niu, Y. Yi, Y. Chen, J. Yuan, J. Zhang, H. Li, Y. Xia, Y. Wang and Z. Deng (2023). Inducible Pluripotent Stem Cell-Derived Small Extracellular Vesicles Rejuvenate Senescent Blood-Brain Barrier to Protect against Ischemic Stroke in Aged Mice. ACS Nano. 17(1): 775-789. DOI:10.1021/acsnano.2c10824

Li, Y. and J. Zhang (2021). Animal models of stroke. Animal Model Exp Med. 4(3):204-219. DOI:10.1002/ame2.12179

Lin, J., Y. Xu, P. Guo, Y. J. Chen, J. Zhou, M. Xia, B. Tan, X. Liu, H. Feng and Y. Chen (2023). CCL5/CCR5-mediated peripheral inflammation exacerbates blood–brain barrier disruption after intracerebral hemorrhage in mice. J Transl Med. 21(1): 196. DOI:10.1186/s12967-023-04044-3

Liu, C., Z. Li and H. Xi (2022). Bioinformatics analysis and *in vivo* validation of ferroptosis-related genes in ischemic stroke. Front Pharmacol. 13: 940260. DOI:10.3389/fphar.2022.940260

Liu, X., L. Fan, J. Li, Z. Bai, Y. Wang, Y. Liu, H. Jiang, A. Tao, X. Li, H. Zhang and N. Tan (2023). Mailuoning oral liquid attenuates convalescent cerebral ischemia by inhibiting AMPK/mTOR-associated apoptosis and promoting CREB/BDNF-mediated neuroprotection. J Ethnopharmacol. 317: 116731. DOI:10.1016/j.jep.2023.116731

Maqoud, F., R. Scala, M. Hoxha, B. Zappacosta and D. Tricarico (2022). ATP-sensitive Potassium Channel Subunits in Neuroinflammation: Novel Drug Targets in Neurodegenerative Disorders. CNS Neurol Disord Drug Targets. 21(2): 130-149. DOI:10.2174/1871527320666210119095626

Meirinho, S., M. Rodrigues, A. Fortuna, A. Falcão and G. Alves (2021). Liquid chromatographic methods for determination of the new antiepileptic drugs stiripentol, retigabine, rufinamide and perampanel: A comprehensive and critical review. J Pharm Anal. 11(4): 405-421. DOI:10.1016/j.jpha.2020.11.005

Mendelson, S. J. and S. Prabhakaran (2021). Diagnosis and Management of Transient Ischemic Attack and Acute Ischemic Stroke: A Review. JAMA. 325(11): 1088-1098. DOI:10.1001/jama.2020.26867

Morisaki, Y., I. Nakagawa, Y. Ogawa, S. Yokoyama, T. Furuta, Y. Saito and H. Nakase (2022). Ischemic Postconditioning Reduces NMDA Receptor Currents Through the Opening of the Mitochondrial Permeability Transition Pore and KATP Channel in Mouse Neurons. Cell Mol Neurobiol. 42(4): 1079-1089. DOI:10.1007/ s10571-020-00996-y

Nass, R. D., C. Kurth, A. Kull, W. Graf, B. Kasper, H. M. Hamer, A. Strzelczyk, C. E. Elger, B. J. Steinhoff, R. Surges and F. Rosenow (2016). Adjunctive retigabine in refractory focal epilepsy: Postmarketing experience at four tertiary epilepsy care centers in Germany. Epilepsy Behav. 56: 54-8. DOI:10.1016/j.yebeh.2015.12.034

Nilsen, N. J., G. I. Vladimer, J. Stenvik, M. P. Orning, M. V. Zeid-Kilani, M. Bugge, B. Bergstroem, J. Conlon, H. Husebye, A. G. Hise, K. A. Fitzgerald, T. Espevik and E. Lien (2015). A role for the adaptor proteins TRAM and TRIF in toll-like receptor 2 signaling. J Biol Chem. 290(6): 3209-22. DOI:10.1074/jbc.M114.593426

Qiu, Y. M., C. L. Zhang, A. Q. Chen, H. L. Wang, Y. F. Zhou, Y. N. Li and B. Hu (2021). Immune Cells in the BBB Disruption After Acute Ischemic Stroke: Targets for Immune Therapy?. Front Immunol. 12: 678744. DOI:10.3389/ fimmu.2021.678744

Song, H., N. Xu and S. Jin (2022). miR-30e-5p attenuates neuronal deficit and inflammation of rats with intracerebral hemorrhage by regulating TLR4. Exp Ther Med. 24(2): 492. DOI:10.3892/etm.2022.11419

Shi, M., J. Chen, T. Liu, W. Dai, Z. Zhou, L. Chen and Y. Xie (2022). Protective Effects of Remimazolam on Cerebral Ischemia/Reperfusion Injury in Rats by Inhibiting of NLRP3 Inflammasome-Dependent Pyroptosis. Drug Des Devel Ther. 16: 413-423. DOI:10.2147/DDDT.S344240

Su, Z., Y. Ye, C. Shen, S. Qiu, Y. Sun, S. Hu, X. Xiong, Y. Li, L. Li and H. Wang (2022). Pathophysiology of Ischemic Stroke: Noncoding RNA Role in Oxidative Stress. Oxid Med Cell Longev. 2022: 5815843. DOI:10.1155/ 2022/5815843

Wanve, M., H. Kaur, D. Sarmah, J. Saraf, K. Pravalika, K. Vats, K. Kalia, A. Borah, D. R. Yavagal, K. R. Dave and P. Bhattacharya (2019). Therapeutic spectrum of interferon-β in ischemic stroke. J Neurosci Res. 97(2): 116-127. DOI:10.1002/jnr.24333

Wei, T., Y. Wang, W. Xu, Y. Liu, H. Chen and Z. Yu (2019). KCa3.1 deficiency attenuates neuroinflammation by regulating an astrocyte phenotype switch involving the PI3K/AKT/GSK3β pathway. Neurobiol Dis. 132: 104588. DOI:10.1016/j.nbd.2019.104588

Xing, Y. and Y. Bai (2020). A Review of Exercise-Induced Neuroplasticity in Ischemic Stroke: Pathology and Mechanisms. Mol Neurobiol. 57(10): 4218-4231. DOI:10.1007/s12035-020-02021-1

Yang, T., S. Zang, Y. Wang, Y. Zhu, L. Jiang, X. Chen, X. Zhang, J. Cheng, R. Gao, H. Xiao and J. Wang (2020). Methamphetamine induced neuroinflammation in mouse brain and microglial cell line BV2: Roles of the TLR4/TRIF/Peli1 signaling axis. Toxicol Lett. 333: 150-158. DOI:10.1016/j.toxlet.2020.07.028

Yokoyama, S., I. Nakagawa, Y. Ogawa, Y. Morisaki, Y. Motoyama, Y. S. Park, Y. Saito and H. Nakase (2019). Ischemic postconditioning prevents surge of presynaptic glutamate release by activating mitochondrial ATP-dependent potassium channels in the mouse hippocampus. PLoS One. 14(4): e0215104. DOI: 10.1371/journal.pone.0215104

Yu, L., Y. Zhang, Q. Chen, Y. He, H. Zhou, H. Wan and J. Yang (2022). Formononetin protects against inflammation associated with cerebral ischemia-reperfusion injury in rats by targeting the JAK2/STAT3 signaling pathway. Biomed Pharmacother. 149: 112836. DOI:10.1016/j.biopha.2022.112836

Zahra, A., R. Liu, J. Wang and J. Wu (2023). Identifying the mechanism of action of the Kv7 channel opener, retigabine in the treatment of epilepsy. Neurol Sci. 44(11): 3819-3825. DOI:10.1007/s10072-023-06955-x

Zhao, Y., X. Zhang, X. Chen and Y. Wei (2022). Neuronal injuries in cerebral infarction and ischemic stroke: From mechanisms to treatment (Review). Int J Mol Med. 49(2): 15. DOI:10.3892/ijmm.2021.5070

Zhang, F., S. Liu, L. Jin, L. Tang, X. Zhao, T. Yang, Y. Wang, B. Huo, R. Liu and H. Li (2020). Antinociceptive Efficacy of Retigabine and Flupirtine for Gout Arthritis Pain. Pharmacology. 105(7-8): 471-476. DOI:10.1159/000505934

Zhou, Z., N. Xu, N. Matei, D. W. McBride, Y. Ding, H. Liang, J. Tang and J. H. Zhang (2021). Sodium butyrate attenuated neuronal apoptosis via GPR41/Gβγ/PI3K/Akt pathway after MCAO in rats. J Cereb Blood Flow Metab. 41(2): 267-281. DOI:10.1177/0271678X20910533.